Enhanced Photocurrent and Dynamic Response in Vertically Aligned In$_2$S$_3$/Ag Core/Shell Nanorod Array Photoconductive Devices

Hilal Cansizoglu,*,[†] Mehmet F. Cansizoglu,[†] Fumiya Watanabe,[§] and Tansel Karabacak[†]
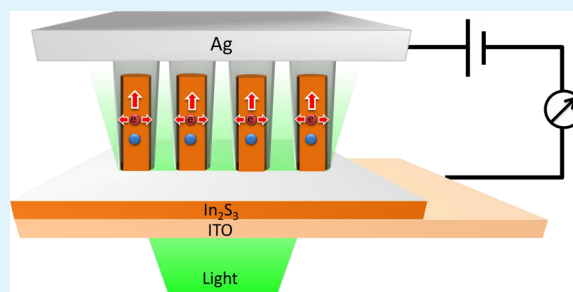
[†]Department of Applied Science, University of Arkansas at Little Rock, Little Rock, Arkansas 72204, United States

[§]Center for Integrative Nanotechnology Sciences, University of Arkansas at Little Rock, Little Rock, Arkansas 72204, United States

S *Supporting Information*

ABSTRACT: Enhanced photocurrent values were achieved through a semiconductor-core/metal-shell nanorod array photoconductive device geometry. Vertically aligned indium sulfide (In$_2$S$_3$) nanorods were formed as the core by using glancing angle deposition technique (GLAD). A thin silver (Ag) layer is conformally coated around nanorods as the metallic shell through a high pressure sputter deposition method. This was followed by capping the nanorods with a metallic blanket layer of Ag film by utilizing a new small angle deposition technique combined with GLAD. Radial interface that was formed by the core/shell geometry provided an efficient charge carrier collection by shortening carrier transit times, which led to a superior photocurrent and gain. Thin metal shells around nanorods acted as a passivation layer to decrease surface states that cause prolonged carrier lifetimes and slow recovery of the photocurrent in nanorods. A combination of efficient carrier collection with surface passivation resulted in enhanced photocurrent and dynamic response at the same time in one device structure. In$_2$S$_3$ nanorod devices without the metal shell and with relatively thicker metal shell were also fabricated and characterized for comparison. In$_2$S$_3$ nanorods with thin metal shell showed the highest photosensitivity (photocurrent/dark current) response compared to two other designs. Microstructural, morphological, and electronic properties of the core/shell nanorods were used to explain the results observed.

KEYWORDS: *core/shell structure, nanowire/nanorod arrays, photoconductivity, glancing angle deposition (GLAD), indium sulfide (In$_2$S$_3$), metal capping*

INTRODUCTION

Efficient photon absorption and charge carrier collection are two major requirements for enhanced photoconductive gain (i.e., number of collected carriers/number of absorbed photons) in semiconductor photodetectors.[1] Semiconducting nanostructures were proven to meet these requirements and became promising candidates in photodetector applications.[2,3] Some of the most encouraging results regarding the use of nanostructures in photosensitive applications incorporated nanowire (NW, also used to refer to the "nanorod" geometry) where a high photoconductive gain can be obtained.[4,5] NW arrays were shown to increase optical absorption even in low quality materials.[6]

Another superiority of NWs compared to thin film counterparts in photodetector applications is their high surface to volume ratio, leading to high density of the surface states. As illustrated in Figure 1, a depletion region due to Fermi level pinning[7] at the surface of the wire can be formed due to the high density of the surface states. Some photoexcited carriers in this region can move toward inside the wire while oppositely charged ones flow to the surface and get trapped there. Charge carriers that move toward the NW interior can reach the current-collecting electrode and circulate the device multiple times before they recombine with the opposite charge carriers

that are trapped at surface states. Thus, an efficient charge separation can be maintained and this can result in significantly reduced surface recombination and prolonged carrier lifetimes.[7] In addition, short interelectrode spacing within NWs allows carriers to transit between electrodes at a faster rate.[7] For a highly light-absorbing material, enhanced photoconductive gain can be obtained mainly through the combination of prolonged carrier lifetimes and reduced transit times. However, high gain is usually received at the expense of dynamic response. NWs with long carrier lifetimes typically suffer from long recovery times and thus show persistent photocurrents.[8−11] Therefore, there is a need for alternative photoconductive device structure approaches to achieve high gain values while maintaining an appropriate dynamic response.

Core−shell nanowire structures were proposed for enhanced photosensitivity[12] and have recently received great attention in photovoltaic and photodetector applications.[13−17] Some of these studies utilized semiconductor materials for both core and shell regions,[14,15] whereas a few others employed a metal core and a semiconductor shell[16] to build nanowire photodetectors.
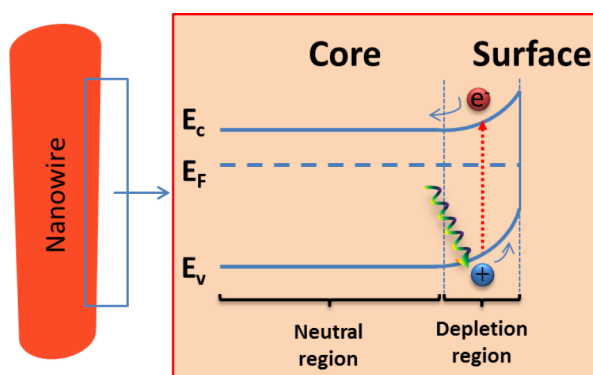
Figure 1. Energy band diagram of a nanowire near its surface under illumination is illustrated. The high density of the surface states causes a depletion region due to Fermi level pinning at the surface of the nanowire. This region provides efficient charge separation; photo-exited electrons are forced to flow to the nanowire core and holes are trapped at the surface. This helps photoexited carriers live longer and makes surface recombination almost impossible.

Fan et al. also demonstrated a single-nanowire photodetector with a silicon core and gold shell.[17] On the other hand, to the best of authors' knowledge, the semiconductor-core/metal-shell structure of vertically aligned NW arrays has not been studied for photodetector applications before. Enhanced photocurrents along with dynamic response in vertically aligned nanorod arrays can potentially be achieved by introducing a thin metal shell around semiconducting nanorods. Densely packed vertically aligned nanorods were proven to trap light effectively inside the nanorod layer and enhance diffuse light scattering, which results in high optical absorption.[5,6] The enhanced interface of the vertically aligned semiconductor-nanorod-core/metal-shell structure can significantly increase contact area and provide efficient carrier collection by introducing additional carrier transportation paths in radial directions.[18,19] This new radial-contact geometry can decrease transit time of excess carriers in nanorods and result in high photoconductive gain even with short carrier lifetimes. In other words, high defect-density low quality semiconductors can potentially be implemented as efficient photodetector materials in a vertically aligned core/shell nanorod array device structure.

Along with the advantages of using vertically aligned NW or nanorod arrays, one of the major drawbacks is encountered during the fabrication of a photoconductive device. Unlike in conventional thin film devices, where metallic contact can simply be deposited on the top surface of a planar semiconducting film, it becomes a challenging task to introduce a similar blanket layer of metal contact on the tips of vertically aligned NW arrays in nanostructured devices.[20–22] During a typical thin film deposition process such as sputtering, incident metal atoms deposit unevenly on the NW array surface, which can lead to device failure. The high aspect ratio of nanowires can cause nonuniform top contacts, or porous structure of the wires may result in short circuit if there is no protection layer between back contact and nanowires. Many of the studies in the literature about nanostructured photodetectors include a single NW and require elaborate fabrication processing steps.[2–4,23–25] A common procedure is to lay down a single nanowire and deposit metal contacts on both ends of the nanowire with the help of lithographical techniques. There are a few reports[26] that also use lithography for laterally aligned nanowire arrays. In addition, there have been some studies that used alternative methods of fabricating contacts on top of wire array structures.[27–30] In the study about vertically aligned Si microwire arrays solar cells,[29] the space between microwires was filled with a transparent, nonconducting, thermoplastic polymer before ITO top contact deposition on microwire arrays. Another study in the literature has utilized a random-network of Al nanowires on top of vertically aligned CdS nanowires.[30]

In addition to these sophisticated NW metallization methods, a simple and unique capping technique has recently been developed,[5,31,32] which evolved from a combination of small angle deposition (SAD)[33–35] and glancing angle deposition (GLAD)[32,36,37] methods (also called oblique angle deposition). The capping process is mainly based on gradually decreasing the incidence angle of atoms coming to the tips of vertical NW/nanorod arrays from glancing to moderate and to normal angles. (See the Experimental Section for details.) This new capping approach can potentially overcome most of the problems associated with fabricating electrical contacts on NW/nanorod array structures.

In this work, arrays of In_2S_3-semiconducting-nanorods/Ag-metal core/shell structures having a uniform top metal contact were utilized to demonstrate enhanced photocurrent and dynamic response of radial-contact photodetector devices. Vertically aligned In_2S_3 nanorods were deposited by GLAD technique and a thin Ag film is coated around In_2S_3 nanorods as the metallic shell by a high pressure sputter deposition method. Capping process was used to deposit a Ag blanket layer on top of In_2S_3 nanorods as the top metal contact. In_2S_3 is an n-type semiconductor with a relatively wide band gap of ~2.0 eV[38,39] and a promising material in photodetection applications.[5,40] For this reason, In_2S_3 nanorods have been used as a model material system in the current study; nevertheless, our approach can be applied to a wide range of NW/nanorod arrays systems as well. In addition, identical nanorods without a metal shell and a relatively thicker shell were also fabricated and tested for comparison. Results indicate that nanorods with a thin shell show enhanced photocurrent (~2-fold increase), shorter temporal response time (~3 times shorter), and superior photosensitivity (photocurrent/dark current, ~3 times higher) compared to the nanorods without a shell. A relatively thick shell is observed to increase the photocurrent, but shows a decrease in photosensitivity due to relatively high dark currents.

■ EXPERIMENTAL SECTION

Fabrication of Nanostructured Photoconductive Device (NPDs). 2.5 × 2.5 cm indium tin oxide (ITO) coated glass (SPI Supplies, 8−12 ohms/square, 700 nm, greater than 83% transparency) was used as the substrate. The active semiconducting layer includes In_2S_3 film and In_2S_3 nanorods in each NPD structure. In_2S_3 thin film is deposited with a thermal evaporation technique on ITO to prevent unwanted contact between ITO and metal contact. In_2S_3 was thermally evaporated to deposit nanorods in the same physical vapor deposition (PVD) system that has a GLAD attachment, which incorporates a substrate modulation for tilt and rotation control. As described in detail elsewhere,[6] GLAD is a simple and effective PVD nanostructure growth technique. During GLAD, incident flux of atoms comes to the surface of a tilted and rotating substrate at highly oblique angles (compared to surface normal), which are typically more than 70°, and form island-like structures at the initial stages. As the growth proceeds, incoming atoms preferentially stick to the tops of islands of higher height due to the "shadowing effect", which leads to the formation of isolated columnar structures. At sufficiently high rotation speeds, this mechanism results in the growth of vertically aligned nanorod arrays.

In$_2$S$_3$ powder (from CERAC) was used as the evaporation source material. Film and nanorod depositions were held at room temperature under 2.0×10^{-6} mbar base pressure with a deposition rate of 0.2 nm/sec (i.e., nanorod length/deposition time), which was measured by quartz crystal microbalance (QCM) and confirmed by the analysis of cross-sectional scanning electron microscopy (SEM, JEOL JSM 7000F) images. For nanorod fabrication, samples were positioned at 85° incidence angle measured between the incident flux and the substrate normal axis. In$_2$S$_3$ nanorods were deposited right after In$_2$S$_3$ thin film growth. After active layer (In$_2$S$_3$ thin film and nanorods) fabrication, samples were taken out of the PVD system and were applied a vacuum compatible plastic shadowing mask that had 6 circular openings (0.08 cm^2) on it to form isolated devices on the same sample. After the mask was attached, samples were put back into the same PVD system to be coated with metal shell and metal capping.

For the structures with a metallic shell, nanorods were coated with Ag by sputtering at high pressure, which is a well-known and widely used technique in the literature, especially in gold coaters for SEM systems. The working gas (Ar) pressure was set to 3.0×10^{-2} mbar in order to achieve a conformal-like metal shell around the nanorods.

For the metal capping, the Ar pressure was reduced to 3.0×10^{-3} mbar, and Ag was sputter deposited on top of nanorods by using a novel capping process. As illustrated in Figure 2, the initial stage of the capping process is basically deposition at glancing angles (i.e., GLAD). Incident flux of metal atoms comes to the substrate surface at a high angle and starts to stick to the tips of the predeposited vertically
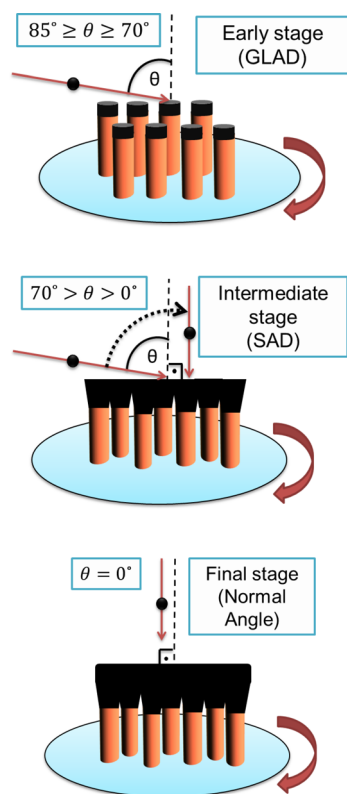
aligned In$_2$S$_3$ nanorod arrays. They continue to grow in the vertical direction due to the combination of shadowing effect and substrate rotation. Then the tilt angle was gradually decreased at a rate of 2°/min and brought the growth a small angle deposition (SAD) regime.[33−35] During the SAD stage, atoms can reach to the sides of the tiny metallic nanorods that are formed at the initial GLAD stage. As illustrated in Figure 2, tiny metallic nanorods evolve to tapered cone-like structures during the intermediate SAD stage of capping process. At small angles, structures start to merge together to form a uniform blanket layer on top of vertically aligned nanorods. The final stage of the capping process (Figure 2) includes conventional deposition at normal angle to introduce a continuous metal film. In this study, Ag was deposited at normal angle for 5 min and about a 700 nm thick metallic layer is formed during deposition (total deposition time including capping is 45 min).

Preparation of TEM Samples. In$_2$S$_3$ nanorods were deposited on Si substrates under the same experimental conditions used in NPD preparation. Then In$_2$S$_3$ nanorods were coated with thin and thick Ag layers in separate depositions with the same deposition technique (high pressure sputtering) and same parameters used for Ag shells in NPDs. After that, Ag coated In$_2$S$_3$ nanorods were scribed off from Si substrate onto TEM grids in order to be analyzed under TEM.

Morphological Characterization. Morphological characterization of Ag covered In$_2$S$_3$ nanorods was done by scanning electron microscopy (SEM, JEOL JSM 7000F) and transmission electron microscopy (TEM, JEOL JEM 2100F). All STEM/EDS images were taken by a 1.5 nm beam size at 80 kV.

Photoconductivity Experiments. A Keithley 2400 sourcemeter with two probes was used for electrical characterization. A laser diode at a 532 nm wavelength (Roithner LaserTechnik, CW 532-005F) was used as a light source in photocurrent measurements. The incidence light intensity was 3 mW/cm^2. A BK Precision 1788 programmable DC power supply was used to control the light source, which was turned on and off in 10 s time intervals.

RESULTS AND DISCUSSION

As-deposited thin film and GLAD nanorods of indium sulfide were found to be stoichiometric In$_2$S$_3$, yet with an amorphous structure.[5] Figure 3a illustrates the device structure without the metal shell, and Figure 3b,c demonstrates the radial-contact NPD structures with relatively thin and thick metallic shells around nanorods, respectively. Figure 3d−f shows SEM images of the NPD structures, which were produced to correspond to device structures of Figure 3a−c, respectively. Figure 3d shows the Ag cap layer, In$_2$S$_3$ nanorods, and In$_2$S$_3$ thin film on ITO coated glass substrate (top to bottom) and the inset indicates a higher resolution SEM image that allows the nanorods and film appear clearly.

The height of the In$_2$S$_3$ nanorods was measured as 198 ± 12 nm and bottom In$_2$S$_3$ film thickness was found to be 57 ± 4 nm by analyzing SEM images. Figure 3e,f shows In$_2$S$_3$ nanorods with a Ag metal shell and underlying In$_2$S$_3$ thin film on the Si substrate (the Ag cap layer was peeled off for convenience). We used SEM images of In$_2$S$_3$ nanorods with a Ag metal shell grown on Si instead of ITO coated glass substrate for convenience of Si substrates during SEM sample preparation. However, we observed that there is no morphological difference in nanorods on Si substrate and the nanorods grown on ITO coated glass substrate, as can be seen in Figure S1b,c (see the Supporting Information). The capping process forms a continuous top metal film (indicated by two-sided arrow) of about 700 nm in thickness, shown in Figure S1a (see the Supporting Information).

Assuming the shape of the nanorods are perfect cylinders and given that the material filling ratio of nanorods (0.7) and Ag deposition rate (30 nm/min), we calculated the estimated

Figure 2. Stages of metal capping process are illustrated. At early stage of the deposition, incident flux comes to the substrate plane at high angles of $70° \leq \theta \leq 85°$ (glancing angle deposition, GLAD) and continues to form columnar metal contacts on top of nanorods. At intermediate stages, flux approaches at relatively small angles of $0° < \theta < 70°$ (small angle deposition, SAD), and that allows atoms to deposit on sides of columnar structure leading to a lateral growth. As the deposition angle is gradually decreased, columnar metal features coalesce and start to form a continuous film. At the final stage, the metal is deposited at normal angle incidence to form a uniform blanket thin film.
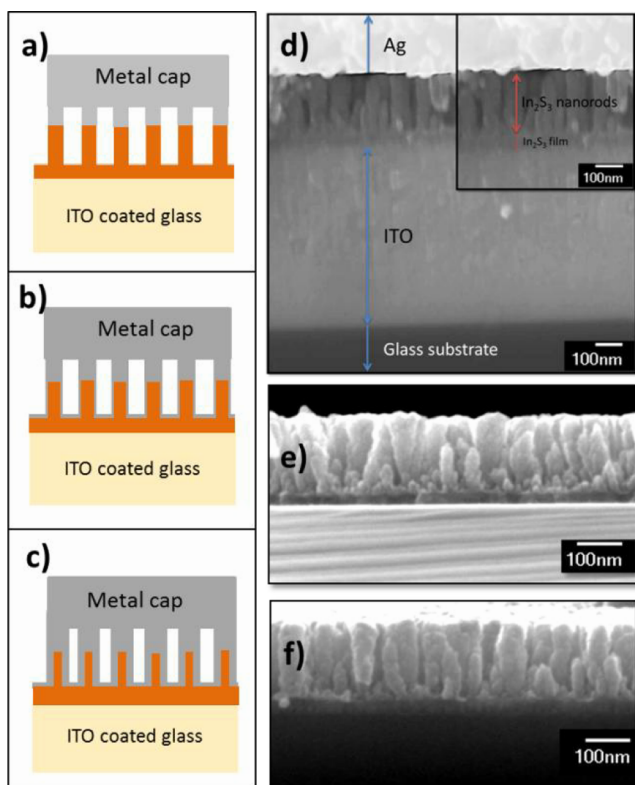
Figure 3. Schematics and SEM images for photoconductive device structures are illustrated. (a) Nanostructured photoconductive device (NPD) structure (control sample, without metallic shell), (b) NPD structure with a thin metallic shell, (c) NPD structure with a relatively thick metallic shell, (d) SEM image of vertically aligned In_2S_3 nanorod arrays and underlying In_2S_3 film on ITO coated glass substrate, with a Ag metallic capping layer on top of nanorods, (e) SEM image of In_2S_3 nanorods coated with thin Ag shell and In_2S_3 film on Si substrate, (f) SEM image of In_2S_3 nanorods coated with a relatively thicker Ag shell and In_2S_3 film on Si substrate. The Ag capping layer was peeled off for panels e and f.

thicknesses of Ag thin and thick shells as 1.9 ± 0.1 nm and 3.8 ± 0.2 nm, respectively. As seen in Figure 3e,f, shapes of In_2S_3 nanorods coated with the Ag shell remained same as the bare ones (Figure 3d), which is thought to be an indication of conformal Ag deposition. To investigate the Ag shell's conformality in more detail and measure the shell thickness more accurately, transmission electron microscopy (TEM) and scanning transmission electron microscopy/energy dispersive spectroscopy (of X-ray) (STEM/EDS) analyses were performed and the results are shown in Figure 4. For TEM and STEM/EDS analyses, In_2S_3 nanorods were deposited on bare Si wafers and covered with thin and thick Ag shells under identical experimental conditions as in the deposition of NPDs of this study, which are described above.

A cluster of In_2S_3 nanorods coated with a thin Ag shell can be seen in Figure 4a. Top and bottom portions of an individual nanorod from this cluster are shown in Figure 4b,c, respectively. The thin Ag shell is measured to be about 2.04 ± 0.61 nm (see the Supporting Information for details) from Figure 4b,c where arrows indicate the thin Ag layer. Because In_2S_3 nanorods in this study are amorphous, no crystal structure is expected to be observed in TEM images. However, an ordered atomic structure can be easily seen in Figure 4b even at the bottom of the nanorod covered with thin Ag layer. This is
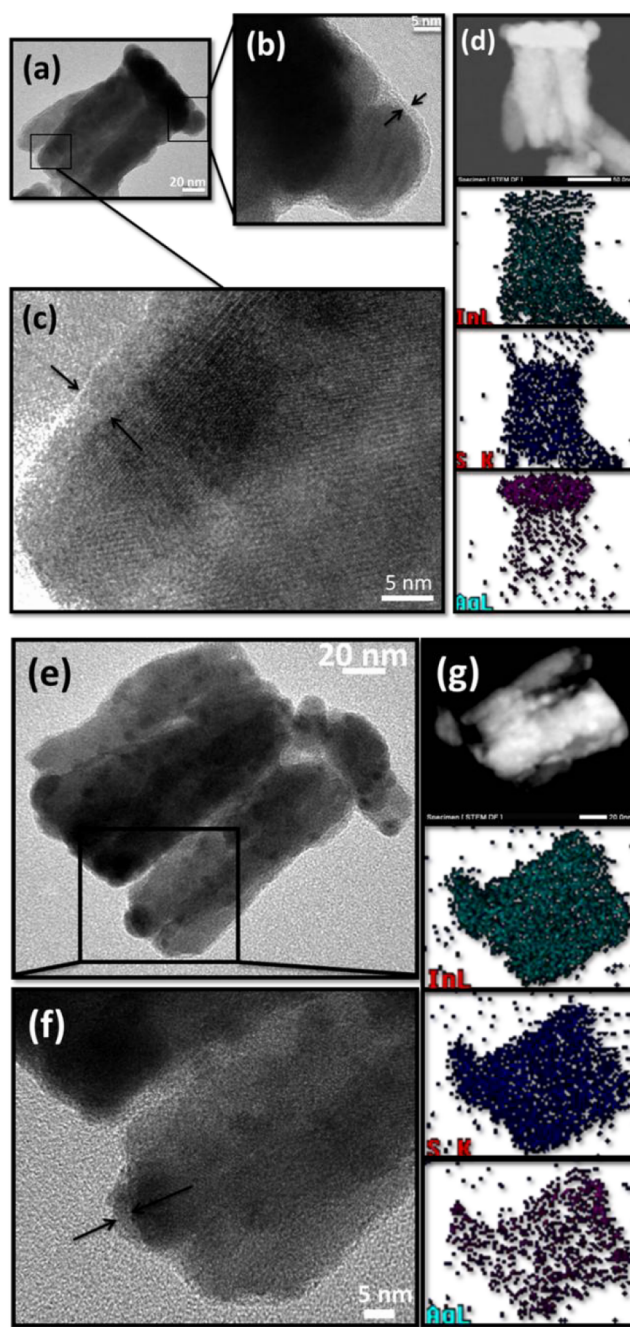

Figure 4. TEM and STEM/EDS images for Ag coated In_2S_3 nanorods are shown. (a) TEM image of a cluster of In_2S_3 nanorods coated with a thin Ag shell (scale bar 20 nm), (b) top portion of an individual Ag coated In_2S_3 nanorod (arrows indicate the thin Ag layer, scale bar 5 nm), (c) bottom portion of an individual Ag coated In_2S_3 nanorod (arrows indicate the Ag layer thickness and ordered atomic structure shows uniform coverage of crystalline Ag around amorphous In_2S_3 nanorods, scale bar 5 nm), (d) STEM image of a cluster of In_2S_3 nanorods coated with a thin Ag shell and EDS indicating the existence of In, S, and Ag throughout the whole nanorod, (e) TEM image of a cluster of In_2S_3 nanorods coated with a thick Ag shell (scale bar 20 nm), (f) top portion of an individual Ag coated In_2S_3 nanorod (arrows indicate the thick Ag layer, scale bar 5 nm), (g) STEM image of a cluster of In_2S_3 nanorods coated with thick Ag shell and EDS indicating uniform distribution of In, S, and Ag along the nanorod.

believed to be a strong indication of uniform Ag coverage around In_2S_3 nanorods. Figure 4d shows a STEM image of the

same cluster of nanorods and associated EDS results indicating the existence of In, S, and Ag throughout the nanorods. It is obvious that Ag is detected along the whole nanorod.

Figure 4e has a TEM image of a group of In_2S_3 nanorods with thick Ag film. The top portion of an individual nanorod with a high magnification is also shown in Figure 4f with arrows pointing the thick Ag shell, which is measured to be about 3.89 ± 0.47 nm (see the Supporting Information for details). The thick shell is found to be almost ∼2 times thicker than the thin shell, which is consistent with the deposition times (i.e., the deposition time of thick shell was 1 min, two times longer than the deposition time of thin shell, which was 30 s). In addition, our estimated shell thicknesses agree well with measured thicknesses from TEM analysis. STEM image and EDS results for In_2S_3 nanorods with thick Ag shell are also shown in Figure 4g, indicating the uniform distribution of In, S, and Ag along the nanorods.

For electrical characterization, we studied current−voltage (I−V) relations for each NPD. I−V curves (not shown here, see the Supporting Information) show an asymmetric behavior, indicating a Schottky interface between In_2S_3 and Ag. However, photoconductivity studies (photo current−time) were performed under forward bias where drift current starts showing linear behavior with applied voltage. We used a green color laser diode (532 nm) to illuminate the devices for photoconductivity measurements. Because In_2S_3 absorbs below ∼600 nm due its band gap[5] and ITO underneath the nanorods mostly absorb at the UV region (<400 nm); a 532 nm laser provides an appropriate energy to excite the carriers in In_2S_3 nanorods. Figure 5 shows photocurrent values at various applied voltages for different device structures and also illustrates energy band diagrams at the In_2S_3/Ag interface. The plot in Figure 5a shows the average of photocurrent values obtained from each individual device (six devices total). As can be seen, the photocurrent in nanostructured devices is directly proportional to applied electrical potential at relatively low voltages, but then saturates or even starts decreasing at higher voltages. Figure 5b,c shows the energy band diagram at the In_2S_3/Ag interface under no bias and forward bias, respectively. The Schottky barrier is shrunk under the forward bias and permits electrons move from semiconductor to metal more easily (linear behavior of the I−V curve, see the Supporting Information). The current rises with extra photoexcited electrons, like in Figure 5d, under light illumination and it is expected to increase with applied bias as observed in Figure 5a.

As seen in Figure 5a, the photocurrent saturates and starts decreasing at high voltages. This result can be attributed to minority carrier injection at high electrical potentials,[41] which is illustrated in Figure 5e. In an n-type photoconductor, photogenerated electrons move with a shorter transit time compared to their lifetimes, so they can circulate between electrodes until they recombine. However, holes in the semiconductor typically have longer transit times than their lifetimes in moderate fields, so they cannot contribute to the current. On the other hand, under high applied fields, holes can be injected from the metal to the semiconductor, which increases the recombination rate with the electrons, and the photogeneration rate becomes insufficient to catch up with this undesired recombination at the metal/semiconductor interface.[42] This results in reduction of majority charge carrier concentration, causing the photocurrent to deviate from the linear behavior of increasing with applied voltage at high electrical potentials. Because the semiconductor/metal interface
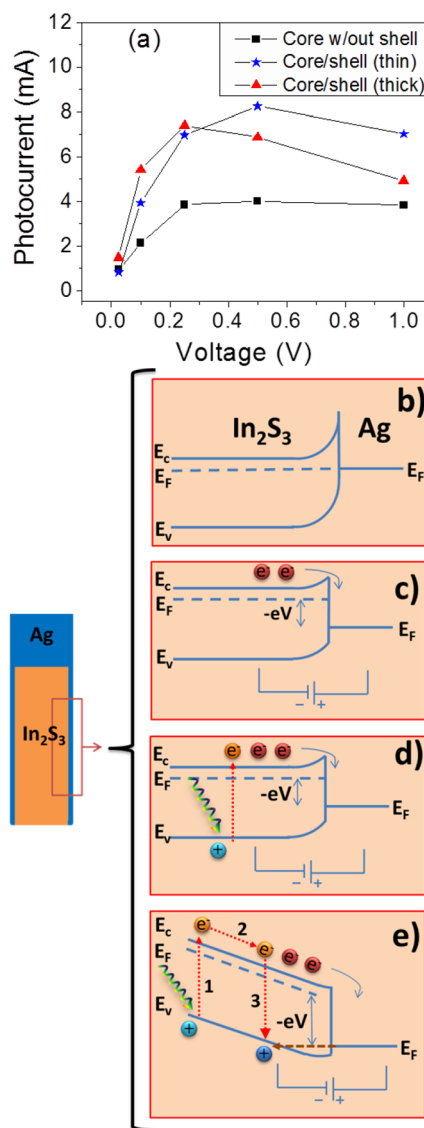

Figure 5. (a) Photocurrent vs applied voltage for different device structures (photocurrent values were obtained from steady-state region of the dynamic photocurrent profiles). Energy band diagram at the semiconductor/metal (In_2S_3/Ag) interface under (b) no bias, (c) forward bias, (d) illuminated forward bias, and (e) illuminated strong forward bias. Under forward bias (c), the Schottky barrier is reduced and that allows electrons to flow from semiconductor to metal more easily. Extra photoexcited carriers contribute to the current under illuminated forward bias condition (d). Strong forward bias (e) causes minority carrier injection (holes, from metal to the semiconductor (orange dashed arrow). Some of the photoexcited electrons (Figure 4e, red dashed arrow, step-1), which would normally contribute to the current (step-2), now recombine with the injected holes (step-3) instead. The photogeneration rate is not fast enough to surpass this recombination at the semiconductor/metal interface and this process results in a reduced photocurrent at a strong forward bias.

is relatively reduced in NPDs without the shell, the photocurrent is least affected among three device structures; however, the photocurrent is dramatically decreased at the larger interface of NPDs with metallic shells.

Figure 5a also allows us to compare photoconductor devices with and without metallic shells in terms of the amount of photocurrent. At moderate fields, the photocurrent in core−shell structures shows ∼2-fold increase compared to the devices

without the shell. The photocurrent could have been enhanced with excess photoexcitation due to higher optical absorption of the device with a metallic shell. However, UV−vis-NIR spectroscopy (with integrating sphere) measurements (see the Supporting Information) indicate that device structures with and without a metal shell absorb light at similar rates (e.g., ∼86% at a 532 nm wavelength). Thus, enhancement in photocurrent can be attributed to reduced transit times, which are thought to be due to shorter interelectrode distances in nanostructured devices with metallic shells. We propose that metallic shells around nanorods help the excess carriers to transit in a short amount of time by introducing alternative pathways in radial directions in addition to the vertical direction along the nanorods. Furthermore, keeping the metal shell thickness small does not seem to have an adverse effect on the overall optical absorption in nanorods, which contributes achieving a high photoconductive gain.

To examine the dynamic behavior of the photocurrent in detail, current was measured as a function of time for each of the six individual devices and the average of the data was plotted for each NPD after subtracting associated dark currents. Figure 6a indicates time dependence of the photocurrent for
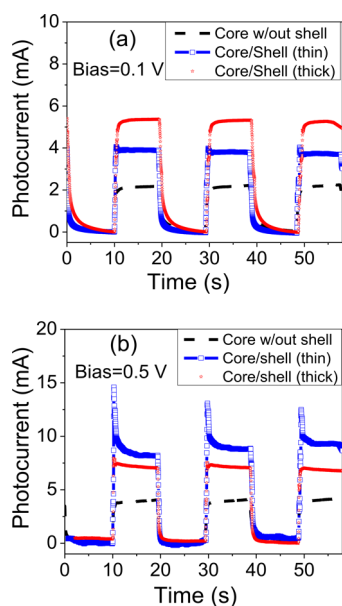

Figure 6. Dynamic photocurrent profiles as the light is turned on (plateaus) and off (valleys) for an applied bias of (a) 0.1 and (b) 0.5 V.

each NPD at 0.1 V bias while the light source was turned on and off at 10 s time intervals. As seen from Figure 6a, NPDs with a thin metal shell show an enhanced photocurrent (∼2-fold increase) compared to NPDs without a metal shell. Similarly, higher photocurrent values were obtained from NPDs with a relatively thick shell compared to other two structures. Enhancement in photocurrent can be attributed to two possible reasons: one is an increase in optical absorption and the second one is efficient carrier transportation and collection. As mentioned above, optical power absorbed in all NPDs was similar to each other. However, UV−vis-NIR spectroscopy measurement results represent optical absorption in the whole device including metal and semiconducting layers. On the other hand, given the fact that loss of light in metals occurs at much smaller rates compared to light absorption in semiconducting materials, and the metal shell thicknesses in our study are

estimated to be in the range of about 2−5 nm, we do not expect a significant change in the amount of the light absorbed in the In_2S_3 regions of different NPDs we used.

Another possible reason for the enhancements in photocurrent can be due to the improved charge carrier collection. If the excess carriers have longer lifetimes than their transit time, they can make more than one circulation through the device until recombination takes place. Therefore, longer lifetimes or shorter transit times can both enhance the photocurrent. To extract photo carrier lifetime, photocurrent decays in Figure 6a (i.e., the sections of the profiles right after the light is turned off) were fitted with an exponential equation that has two decaying components:

$$I = A_1 e^{-t/\tau_{fast}} + A_2 e^{-t/\tau_{slow}} \tag{1}$$

where τ_{fast} and τ_{slow} are the time constants for fast and slow decaying of photocurrent profiles, indicating at least two trap levels. We obtained weight-averaged fast and slow time constants from each decay portions of the profiles shown in Figure 6a. We extracted carrier lifetime from the mean of weight-averaged time constants for each NPD (see the Supporting Information for details). Thus, carrier lifetimes were calculated as 1.07, 0.58, and 0.68 s for NPDs without a metal shell, with a thin metal shell, and with a thick metal shell, respectively. Photo carrier lifetimes for NPDs with a metal shell are found to be lower than NPDs without a shell. However, it can be seen that NPDs with a metal shell had a higher photocurrent response at 0.1 V compared to the one without a shell, although its photo carrier lifetimes were much smaller.

The second parameter that can play an important role in enhancing photocurrent is carrier transit time, which mainly depends on carrier mobility and interelectrode separation. The ratio of carrier lifetime and carrier transit time gives the amount of photoconductive gain, which is defined as number of excess electrons per number of absorbed photons. This definition can be rewritten as

$$G = \frac{I_{ph}/e}{P_{abs}/\hbar\omega} \tag{2}$$

where G is the photoconductive gain, I_{ph} is the photocurrent, e is one electron charge, P_{abs} is the absorbed optical power, and $\hbar\omega$ is the energy of one photon. According to this relation, photoconductive gain values at 0.1 V for NPDs without a shell, with a thin shell, and with a thick shell were calculated as 24.15, 44.36, and 61.06 and corresponding transit times were calculated as 4.44×10^{-2}, 1.3×10^{-2}, and 1.1×10^{-2} s, respectively. Carrier transit times for NPDs with a metal shell are very close to each other and ∼4 times shorter than transit time of carriers in NPDs without a shell. Therefore, despite the reduced charge carrier lifetimes, NPDs with a metal shell show a high photocurrent response, mainly due to the short transit times achieved by the core−shell geometry.

High surface to volume ratio in nanowire/nanorod structures compared to thin film counterparts increase surface states, which are believed to be the main reason for prolonged lifetimes in nanowire/nanorod structures.[7] In_2S_3 nanorods were already shown to have higher photoresponse than their thin film counterparts.[5] In the current study, results from the analysis of photocurrent decay reveal that thin metal shell around nanorods shortens the carrier lifetime. This result suggests that thin metal shell may passivate dangling bonds on the surface of the nanorods and thus decrease the amount of

Table 1. Dark Current, Photocurrent, Photosensitivity (Photocurrent/Dark Current), Temporal Response Time, Gain, and Responsivity (Photocurrent/Optical Power) Values Listed for Each NPD at 0.025, 0.1, 0.25, 0.5, and 1 V Applied Bias and under 532 nm Wavelength Light with an Intensity of 3 mW/cm^2

applied bias (V)	structures	dark current (I_d) (mA)	photo current (I_{ph}) (mA)	$I_{ph}\backslash I_d$ (%)	temporal response time (s)	gain	responsivity (A/W)
0.025	no shell	1.19	0.94	79	2.98	10.64	4.58
	thin shell	0.28	0.81	285	0.56	9.19	3.95
	thick shell	0.8	1.52	190	1.59	17.14	7.37
0.100	no shell	7.02	2.14	31	3.16	24.15	10.38
	thin shell	1.70	3.93	231	1.05	44.36	19.08
	thick shell	5.44	5.41	100	2.44	61.06	26.26
0.250	no shell	20.60	3.85	19	2.64	43.42	18.67
	thin shell	10.50	6.97	66	0.52	78.68	33.83
	thick shell	22.55	7.40	33	1.20	83.54	35.92
0.500	no shell	47.61	4.00	8	1.31	45.15	19.42
	thin shell	32.70	8.25	25	0.15	93.13	40.05
	thick shell	58.92	6.87	12	0.65	77.55	33.35
1.000	no shell	107.02	2.98	3	0.90	33.64	19.42
	thin shell	87.26	7.02	8	0.50	79.25	34.08
	thick shell	117.82	4.93	4	0.46	55.65	23.93

surface states. Therefore, shortening of carrier lifetime may be a result of less surface states.

Figure 6b shows a comparison of photocurrent profiles among each NPD as a function of time at 0.5 V applied voltage. As seen in Figure 6b, transient photocurrent spikes are observed for NPDs with a metal shell. However, the shape of the spike in NPDs with a thin metal shell is sharper than the one in NPDs with a thick metal shell. Initially, the photocurrent reaches its peak value in a very short time (~0.24 s), but then starts decaying and shows a steady-state behavior after a while. A transient photocurrent under illumination is believed to be due to trap states (i.e., defects) at the metal/semiconductor interface.[43] Although there is a strong indication of surface passivation by the metal, defect formation at the semiconductor/metal interface is inevitable during metal shell deposition. Such defects can act like trap states for photoexcited carriers (surface states in In_2S_3 nanorods without a shell, which was described above, were traps for holes such that electrons could move to electrodes easily). Defects at semiconductor/metal interface can also exist in In_2S_3 nanorods without a shell (interface between Ag cap layer and the tips of the In_2S_3 nanorods); however, the photocarrier generation rate overcomes such traps, which are believed to be very limited compared to the ones in Ag coated In_2S_3 nanorods (due to high surface area). Magnitudes of the transient photocurrent in Figure 6b are observed to be decreasing in time. This indicates that a number of electrons trapped in the defects after the first light pulse stay trapped and do not contribute to the photocurrent for the second pulse.[44] Therefore, the peak current becomes lower after the second pulse of light. Trapped electrons need more time than the light pulse interval used in this study (10 s) to be completely released and maintain the same peak current for each pulse.

Although carrier lifetime is shortened in In_2S_3 nanorods with a metal shell, existence of the metal shell helps carriers reach the electrode faster compared to the case without a metal shell. Thus, carriers can circulate multiple times through the device and lead to enhanced gain even with shorter lifetimes. On the other hand, shortening lifetime also helps device to provide faster dynamic response. In Table 1, temporal response, which is defined as the time it takes for the photocurrent to drop down to 90% of its initial value during the decay period after

the light is turned off, are shown along with other parameters for each NPD at various applied bias values. For example, the temporal response time for NPDs with a thinner metal shell at 0.1 V was calculated to be 1.05 s. This is about 3 times shorter than the one for NPDs without a shell, which is believed to be due to the shorter times for recombination in NPDs with a thin metallic shell. While NPDs without a shell show persistent photocurrents, a metal shell allows the photocurrent to diminish easily with the help of short carrier lifetimes. These results demonstrate that an enhanced photocurrent along with faster dynamic response can be accomplished in one photodetector device at the same time by introducing a thin metal shell around the nanorod.

Figure 7 presents the results for photosensitivity (the ratio of photocurrent to dark current) for each NPD at different applied bias values, and also its dynamic change at 0.1 and 0.5 V as the light is sequentially turned on and off. As can be seen in Figure 7a, all NPDs show a similar trend: high photosensitivity at low voltages that drastically decreases with increased applied bias. One of the reasons of this behavior can be attributed to the low photocurrents at relatively high fields due to the effect of minority carrier injection, which was explained above. Another reason is the high dark current values at higher voltages. If photosensitivity among NPDs is compared with each other, one can see that NPDs with a thin metal shell are ~3-fold and ~1.5-fold more sensitive to the light compared to NPDs without a shell and NPDs with a relatively thick metal shell, respectively.

Figure 7b,c indicates dynamic photosensitivity response for each NPD at 0.1 and 0.5 V, respectively, as the light is sequentially turned on and off. The overall behavior of dynamic photosensitivity profiles at 0.5 V plotted in Figure 7c seems similar to the photocurrent response observed in Figure 6b. This is an expected result, as photosensitivity is linearly proportional to photocurrent. However, we cannot see the similar correlation between photocurrent responses and photosensitivity at 0.1 V in Figures 6a and 7b, respectively. Although NPDs with a thick shell have a higher photocurrent at 0.1 V applied bias, their photosensitivity is drastically lower than the sensitivity of NPDs with a thin shell, as seen in Figure 7b.
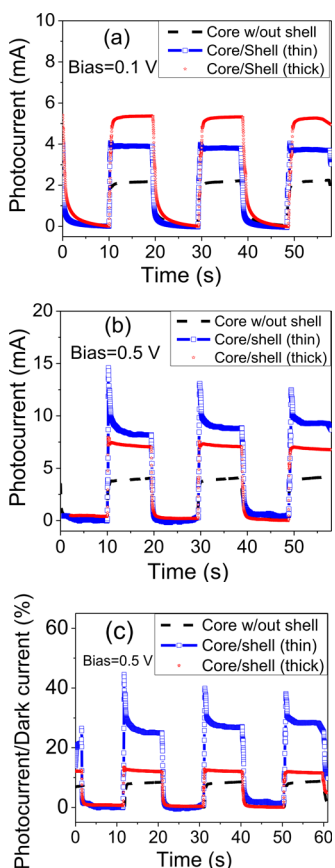
Figure 7. (a) Photosensitivity (the ratio of photocurrent to dark current) at different applied voltages. Dynamic photosensitivity response for each NPD structure at (b) 0.1 V and (c) 0.5 V.

Figure 8. (a) Dark current values at various applied bias for each NPD. NPDs with a thin metal shell show lower dark currents compared to the NPDs with a thicker shell. (b) Wider angular distribution of incident flux at high pressure sputter deposition is illustrated on the left. A zoom-out image of the corner of a nanorod with a metal shell is shown on the right side of the schematic. Atoms that come at oblique angles to the tips of nanorod (indicated as 1) form a columnar structure due to local shadowing effect. Atoms that are able to reach to the side walls of the nanorods (indicated as 2) mainly come at oblique angles with respect to local surface normal. Obliquely coming flux can form a columnar structure also at the side walls of nanorods. This noncontinuous coating can result in high resistance and hence lower dark current values in NPDs with a thin metal shell.

Enhanced sensitivity of NPDs with a thin metal shell compared to NPDs without a shell is expected and can be explained due to enhanced photocurrent in this structure, as seen in Figure 5a. On the other hand, despite their high photocurrents (especially at low voltages), NPDs with a thick metal shell are less sensitive compared to NPDs with a thin metal shell. This enhanced photosensitivity in NPDs with a thin metal shell is mainly due to its low dark current. However, introducing metal around nanorods is normally expected to decrease the total resistance, hence increasing the dark current passing through device. As seen from Figure 8a, this is the case for NPDs with a relatively thick metal shell. Dark current values at different applied voltages for NPDs with a thick shell are higher than dark current values for NPDs without a metal shell. On the other hand, lower dark current values were measured for NPD with a thin metallic shell, even lower compared to NPDs without a shell. This unexpected result can be attributed to microstructural effects introduced during high pressure sputter deposition of the Ag shell.

As shown in Figure 8b, incoming flux of Ag atoms at high pressure sputter deposition has a wider angular distribution. Therefore, some of the incoming atoms can come to the top surface of nanorods at high angles (indicated as 1 in Figure 8b) and can disrupt uniform structure and cause columnar structure formation due to local shadowing effect. In addition, incident atoms coming to the surface at normal and near-normal angles reach the side walls of the nanorods at high angles (indicated as 2 in Figure 8b). They can form columnar structures on the side walls also due to the shadowing effect. Therefore, a slightly
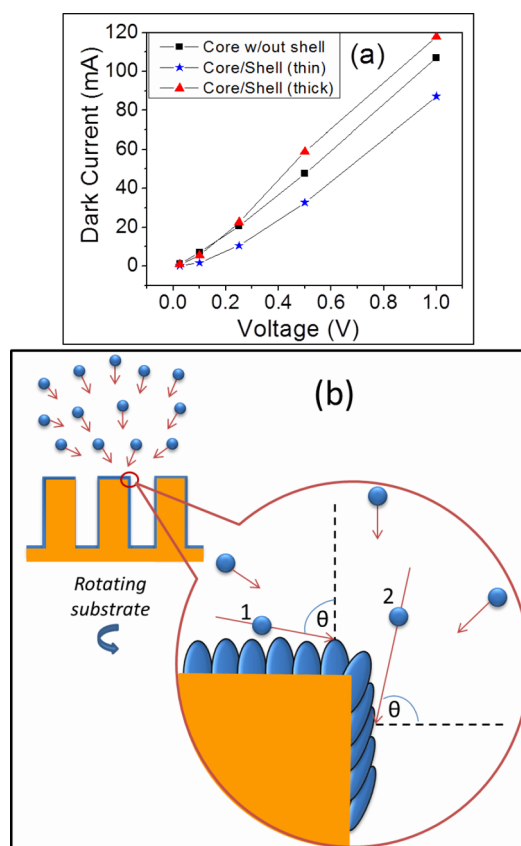
noncontinuous columnar coating around nanorods is thought to be formed, which can result in highly resistive spots in NPDs with a thin metallic shell. On the other hand, as the growth continues, columns can merge and form a more continuous film microstructure, as in the case of NPDs with a thicker shell, which can explain the higher dark current values observed. Therefore, although a thin metal shell lacks high uniformity and hence shows high resistance, this property turns out to be an advantage in photodetector applications of photoconductors where low dark current values are desired.

High dark resistance of a thin shell also affects the behavior of the photocurrent. NPDs with a thin shell produce lower photocurrents than NPDs with a thick shell at moderate applied bias (Figure 5a). We propose that this is due to low resistance of a thick shell as a result of high film uniformity. On the other hand, photocurrent values of NPDs with a thick shell get lower than the photocurrent produced by NPDs with a thin shell under strong forward bias. We propose that low resistance of NPDs with a thick shell causes higher minority carrier injection than that of NPDs with a thin shell, which causes a

8680

dx.doi.org/10.1021/am501481w | ACS Appl. Mater. Interfaces 2014, 6, 8673–8682

more notable decrease in the photocurrent of NPDs with the thick shell.

CONCLUSION

Nanostructured photodetector devices made of vertically aligned indium sulfide nanorod arrays were proven to have enhanced photocurrents along with improved dynamic response by introducing a thin silver metal shell around nanorods. Identical In_2S_3 nanorods without a metal shell and a relatively thick shell were also fabricated and characterized for comparison. Results indicate that the nanorods with a thin metal shell show enhanced photocurrent (∼2-fold increase) and photosensitivity (∼3 times higher) compared to the nanorods without a metal shell. A thin metal shell is thought to passivate the surface states, which in turn reduces the carrier lifetimes and results in superior dynamic response compared to nanorods without a shell. On the other hand, reduced carrier transit time due to short interelectrode spacing compensates the disadvantage of short carrier lifetime and gives rise to the enhanced photoconductive gain and photocurrent. In addition, low dark current values observed in nanorods with a thin metal shell, which is believed to be due to columnar microstructure formed during high pressure sputter deposition of Ag, have led to improved photosensitivity response of the photodetector. On the other hand, a relatively thicker metal shell caused higher dark currents due to a more continuous film microstructure, which resulted in lower photosensitivity response compared to the device with a thinner shell. Our results demonstrate that high photoconductive gain and fast dynamic response can be accomplished in a given device at the same time, even for the ones made of low quality materials with high defect densities.

We propose that our simple device fabrication route, which includes nanostructure layer formation with GLAD, conformal coating by high pressure sputter deposition, and a unique capping process (combination of SAD and GLAD) for top-contact formation, is a promising alternative for potential applications such as detectors, sensors, and imaging devices. Although the device size reported here (0.08 cm^2) is small enough on a research scale but quite large for some potential applications, one can consider lithographical techniques to form smaller isolated devices in order to get dense micro/nano arrays.

ASSOCIATED CONTENT

Ⓢ Supporting Information

Additional SEM images of NPDs without a shell; Ag shell thickness measurement with TEM Analysis; I−V curves of NPD under dark and illuminated conditions; estimation of carrier lifetimes by photocurrent decays. This material is available free of charge via the Internet at http://pubs.acs.org.

AUTHOR INFORMATION

Corresponding Author

*H. Cansizoglu. E-mail: hxis@ualr.edu.

Author Contributions

The paper was written through contributions of all authors. All authors have given approval to the final version of the paper.

Notes

The authors declare no competing financial interest.

REFERENCES

(1) Zhai, T. Y.; Fang, X. S.; Liao, M. Y.; Xu, X. J.; Zeng, H. B.; Yoshio, B.; Golberg, D. A Comprehensive Review of One-Dimensional Metal-Oxide Nanostructure Photodetectors. *Sensors-Basel* **2009**, *9* (8), 6504−6529.

(2) Law, J. B. K.; Thong, J. T. L., Simple Fabrication of a ZnO Nanowire Photodetector with a Fast Photoresponse Time. *Appl. Phys. Lett.* **2006**, *88* (13).

(3) Zhai, T. Y.; Fang, X. S.; Liao, M. Y.; Xu, X. J.; Li, L.; Liu, B. D.; Koide, Y.; Ma, Y.; Yao, J. N.; Bando, Y.; Golberg, D. Fabrication of High-Quality In_2Se_3 Nanowire Arrays toward High-Performance Visible-Light Photodetectors. *ACS Nano* **2010**, *4* (3), 1596−1602.

(4) Soci, C.; Zhang, A.; Xiang, B.; Dayeh, S. A.; Aplin, D. P. R.; Park, J.; Bao, X. Y.; Lo, Y. H.; Wang, D. ZnO Nanowire UV Photodetectors with High Internal Gain. *Nano Lett.* **2007**, *7* (4), 1003−1009.

(5) Cansizoglu, M. F.; Engelken, R.; Seo, H. W.; Karabacak, T. High Optical Absorption of Indium Sulfide Nanorod Arrays Formed by Glancing Angle Deposition. *ACS Nano* **2010**, *4* (2), 733−740.

(6) Cansizoglu, H.; Cansizoglu, M. F.; Finckenor, M.; Karabacak, T. Optical Absorption Properties of Semiconducting Nanostructures with Different Shapes. *Adv. Opt. Mater.* **2013**, *1* (2), 158−166.

(7) Soci, C.; Zhang, A.; Bao, X. Y.; Kim, H.; Lo, Y.; Wang, D. L. Nanowire Photodetectors. *J. Nanosci. Nanotechnol.* **2010**, *10* (3), 1430−1449.

(8) Calarco, R.; Marso, M.; Richter, T.; Aykanat, A. I.; Meijers, R.; Hart, A. V.; Stoica, T.; Luth, H. Size Dependent Photoconductivity in MBE Grown GaN Nanowires. *Nano Lett.* **2005**, *5* (5), 981−984.

(9) Han, S.; Jin, W.; Zhang, D. H.; Tang, T.; Li, C.; Liu, X. L.; Liu, Z. Q.; Lei, B.; Zhou, C. W. Photoconduction Studies on GaN Nanowire Transistors under UV and Polarized UV Illumination. *Chem. Phys. Lett.* **2004**, *389* (1−3), 176−180.

(10) Salfi, J.; Philipose, U.; de Sousa, C. F.; Aouba, S.; Ruda, H. E. Electrical Properties of Ohmic Contacts to ZnSe Nanowires and Their Application to Nanowire-Based Photodetection. *Appl. Phys. Lett.* **2006**, *89* (26), 261112−261112-3.

(11) Park, J.; Lee, E.; Lee, K. W.; Lee, C. E. Electrical Transport and Quasipersistent Photocurrent in Vanadium Oxide Nanowire Networks. *Appl. Phys. Lett.* **2006**, *89* (18), 183114−183114-3.

(12) Hayden, O.; Agarwal, R.; Lieber, C. M. Nanoscale Avalanche Photodiodes for Highly Sensitive and Spatially Resolved Photon Detection. *Nat. Mater.* **2006**, *5* (5), 352−356.

(13) Adachi, M. M.; Anantram, M. P.; Karim, K. S. Optical Properties of Crystalline-Amorphous Core-Shell Silicon Nanowires. *Nano Lett.* **2010**, *10* (10), 4093−4098.

(14) Wang, K.; Chen, J. J.; Zeng, Z. M.; Tarr, J.; Zhou, W. L.; Zhang, Y.; Yan, Y. F.; Jiang, C. S.; Pern, J.; Mascarenhas, A. Synthesis and Photovoltaic Effect of Vertically Aligned ZnO/ZnS Core/Shell Nanowire Arrays. *Appl. Phys. Lett.* **2010**, *96* (12), 123105−123105-3.

(15) Gallo, E. M.; Chen, G. N.; Currie, M.; McGuckin, T.; Prete, P.; Lovergine, N.; Nabet, B.; Spanier, J. E. Picosecond Response Times in GaAs/AlGaAs Core/Shell Nanowire-based Photodetectors. *Appl. Phys. Lett.* **2011**, *98* (24), 241113−241113-3.

(16) Hsu, C. Y.; Lien, D. H.; Lu, S. Y.; Chen, C. Y.; Kang, C. F.; Chueh, Y. L.; Hsu, W. K.; He, J. H. Supersensitive, Ultrafast, and Broad-Band Light-Harvesting Scheme Employing Carbon Nanotube/ TiO_2 Core-Shell Nanowire Geometry. *ACS Nano* **2012**, *6* (8), 6687−6692.

(17) Fan, P. Y.; Chettiar, U. K.; Cao, L. Y.; Afshinmanesh, F.; Engheta, N.; Brongersma, M. L. An Invisible Metal-Semiconductor Photodetector. *Nat. Photonics* **2012**, *6* (6), 380−385.

(18) Kelzenberg, M. D.; Putnam, M. C.; Turner-Evans, D. B.; Lewis, N. S.; Atwater, H. A. Predicted Efficiency of Si Wire Array Solar Cells. *34th IEEE Photovoltaic Specialists Conference (PVSC)*, Philadelphia, PA, June 7−12, 2009; pp 001948−001953.

(19) Kelzenberg, M. D.; Boettcher, S. W.; Petykiewicz, J. A.; Turner-Evans, D. B.; Putnam, M. C.; Warren, E. L.; Spurgeon, J. M.; Briggs, R. M.; Lewis, N. S.; Atwater, H. A. Enhanced Absorption and Carrier Collection in Si Wire Arrays for Photovoltaic Applications. *Nat. Mater.* **2010**, *9* (4), 368−368.

(20) Kim, C. H.; Myung, Y.; Cho, Y. J.; Kim, H. S.; Park, S. H.; Park, J.; Kim, J. Y.; Kim, B. Electronic Structure of Vertically Aligned Mn-Doped $CoFe_2O_4$ Nanowires and Their Application as Humidity Sensors and Photodetectors. *J. Phys. Chem. C* **2009**, *113* (17), 7085−7090.

(21) Kushwaha, A.; Aslam, M. Defect Induced High Photocurrent in Solution Grown Vertically Aligned ZnO Nanowire Array Films. *J. Appl. Phys.* **2012**, *112* (5), 054316−054316-7.

(22) Chinnamuthu, P.; Dhar, J. C.; Mondal, A.; Bhattacharyya, A.; Singh, N. K. Ultraviolet Detection using TiO_2 Nanowire Array with Ag Schottky Contact. *J. Phys. D: Appl. Phys.* **2012**, *45* (13), 135102.

(23) Heo, Y. W.; Kang, B. S.; Tien, L. C.; Norton, D. P.; Ren, F.; La Roche, J. R.; Pearton, S. J. UV Photoresponse of Single ZnO Nanowires. *Appl. Phys. A: Mater. Sci. Process.* **2005**, *80* (3), 497−499.

(24) Chen, L. C.; Huang, H. M.; Chen, R. S.; Chen, H. Y.; Liu, T. W.; Kuo, C. C.; Chen, C. P.; Hsu, H. C.; Chen, K. H.; Yang, Y. J. Photoconductivity in Single AlN Nanowires by Subband Gap Excitation. *Appl. Phys. Lett.* **2010**, *96* (6), 062104−062104-3.

(25) Gu, Y.; Romankiewicz, J. P.; David, J. K.; Lensch, J. L.; Lauhon, L. J.; Kwak, E. S.; Odom, T. W. Local Photocurrent Mapping as a Probe of Contact Effects and Charge Carrier Transport in Semiconductor Nanowire Devices. *J. Vac. Sci. Technol., B: Microelectron. Nanometer Struct.−Process., Meas., Phenom.* **2006**, *24* (4), 2172−2177.

(26) Peng, S. M.; Su, Y. K.; Ji, L. W.; Wu, C. Z.; Cheng, W. B.; Chao, W. C. ZnO Nanobridge Array UV Photodetectors. *J. Phys. Chem. C* **2010**, *114* (7), 3204−3208.

(27) Senanayake, P.; Hung, C. H.; Shapiro, J.; Lin, A.; Liang, B. L.; Williams, B. S.; Huffaker, D. L. Surface Plasmon-Enhanced Nanopillar Photodetectors. *Nano Lett.* **2011**, *11* (12), 5279−5283.

(28) Senanayake, P.; Lin, A.; Mariani, G.; Shapiro, J.; Tu, C.; Scofield, A. C.; Wong, P. S.; Liang, B. L.; Huffaker, D. L. Photoconductive Gain in Patterned Nanopillar Photodetector Arrays. *Appl. Phys. Lett.* **2010**, *97* (20), 203108−203108-3.

(29) Putnam, M. C.; Boettcher, S. W.; Kelzenberg, M. D.; Turner-Evans, D. B.; Spurgeon, J. M.; Warren, E. L.; Briggs, R. M.; Lewis, N. S.; Atwater, H. A. Si Microwire-Array Solar Cells. *Energy Environ. Sci.* **2010**, *3* (8), 1037−1041.

(30) Azulai, D.; Givan, U.; Shpaisman, N.; Belenkova, T. L.; Gilon, H.; Patolsky, F.; Markovich, G. On-Surface Formation of Metal Nanowire Transparent Top Electrodes on CdSe Nanowire Array-Based Photoconductive Devices. *ACS Appl. Mater. Interfaces* **2012**, *4* (6), 3157−3162.

(31) Xi, J. Q.; Kim, J. K.; Schubert, E. F.; Ye, D. X.; Lu, T. M.; Lin, S. Y.; Juneja, J. S. Very Low-Refractive-Index Optical Thin Films Consisting of an Array of SiO2 Nanorods. *Opt. Lett.* **2006**, *31* (5), 601−603.

(32) Robbie, K.; Brett, M. J. Sculptured Thin Films and Glancing Angle Deposition: Growth Mechanics and Applications. *J. Vac. Sci. Technol., A* **1997**, *15* (3), 1460−1465.

(33) Khudhayer, W. J.; Kariuki, N.; Myers, D. J.; Shaikh, A. U.; Karabacak, T. GLAD Cr Nanorods Coated with SAD Pt Thin Film for Oxygen Reduction Reaction. *J. Electrochem. Soc.* **2012**, *159* (6), B729−B736.

(34) Karabacak, T.; Lu, T. M. Enhanced Step Coverage by Oblique Angle Physical Vapor Deposition. *J. Appl. Phys.* **2005**, *97* (12), 124504.

(35) Karabacak, T.; Lu, T.-M. Enhanced Step Coverage of Thin Films on Patterned Substrates by Oblique Angle Physical Vapor Deposition. U.S. Patent No: 7,244,670, July 17, 2007.

(36) Karabacak, T.; Lu, T.-M. Shadowing Growth and Physical Self-Assembly of 3D Columnar Structures. In *Handbook of Theoretical and Computational Nanotechnology*; Rieth, M.; Schommers, W., Eds.; American Scientific Publishers: Stevenson Ranch, CA, 2005; Chapter 69, p 729.

(37) Robbie, K.; Brett, M. J.; Lakhtakia, A. Chiral Sculptured Thin Films. *Nature* **1996**, *384* (6610), 616−616.

(38) Yoosuf, R.; Jayaraj, M. K. Optical and Photoelectrical Properties of Beta-In_2S_3 Thin Films Prepared by Two-Stage Process. *Sol. Energy Mater. Sol. Cells* **2005**, *89* (1), 85−94.

(39) Pathan, H. M.; Lokhande, C. D.; Kulkarni, S. S.; Amalnerkar, D. P.; Seth, T.; Han, S. H. Some Studies on Successive Ionic Layer Adsorption and Reaction (SILAR) Grown Indium Sulphide Thin Films. *Mater. Res. Bull.* **2005**, *40* (6), 1018−1023.

(40) Tang, J.; Konstantatos, G.; Hinds, S.; Myrskog, S.; Pattantyus-Abraham, A. G.; Clifford, J.; Sargent, E. H. Heavy-Metal-Free Solution-Processed Nanoparticle-Based Photodetectors: Doping of Intrinsic Vacancies Enables Engineering of Sensitivity and Speed. *ACS Nano* **2009**, *3* (2), 331−338.

(41) Kao, K. C. *Dielectric Phenomena in Solids*; Elsevier Academic Press: Amsterdam, 2004.

(42) Sze, S. M.; Ng, K. K. *Physics of Semiconductor Devices*, Third ed.; John Wiley & Sons, Inc.: New York, 2001; p 669.

(43) Mayer, M. T.; Du, C.; Wang, D. W. Hematite/Si Nanowire Dual-Absorber System for Photoelectrochemical Water Splitting at Low Applied Potentials. *J. Am. Chem. Soc.* **2012**, *134* (30), 12406−12409.

(44) Lacaita, A.; Francese, P. A.; Zappa, F.; Cova, S. Single-Photon Detection Beyond 1mm: Performance of Commercially Available Germanium Photodiodes. *Appl. Opt.* **1994**, *33* (30), 6902−6918.